Available online freely at www.isisn.org

Bioscience Research

Print ISSN: 1811-9506 Online ISSN: 2218-3973

Journal by Innovative Scientific Information & Services Network

RESEARCH ARTICLE BIOSCIENCE RESEARCH, 2024 21(1):35-54. **OPEN ACCESS**

Ligational behaviour of tridentate NNO-donor Schiff base incorporating imidazole moiety towards V(III), Mn(II), Co(II), Ni(II), and Zn(II) ions preparation, characterisation, antitumor, and antimicrobial investigation

Ahmed Noman Al-Hakemi[1,2,*], Tahini Meataq Alresheedi[1], Reema Ali Albarrak[1] , Mohamed Mahmoud Shakdofa[3], Abuzar Ebead Albadri[1,4], Marwa Mohamed Abd El-Hady[1,5]and Saeed El-Sayed Saeed[1]

[1]Department of Chemistry, College of Science, Qassim University, Buraidah 51452, **Saudi Arabia**
[2]Department of Chemistry, Faculty of Science, Ibb University, Ibb, **Yemen**
[3]Inorganic Chemistry Department, National Research Centre, El-booth St., Doka, Cairo, **Egypt**
[4]Department of Chemistry, Faculty of Science, University of Khartoum. PO Box 321 Khartoum, **Sudan**
[5]National Research Centre, Institute of Textile Research and Technology, Dokki, Giza P.O. Box 12622, **Egypt**

***Correspondence:** A.Alhakimi@qu.edu.sa, Alhakemi10@yahoo.com **Received 15 Oct., 2023, Revised: 28 December 2023, Accepted: 31 December 2023 e-Published: 07 January 2024**

V(III), Mn(II), Co(II), Ni(II), and Zn(II) complexes of NNO donor Schiff base named 4- ((((1H-benzo[d]imidazol-2-yl)methyl)imino)methyl)benzene-1,3-diol(HL)were synthesised and structurally elucidated based on analytical, thermal (DTA, TGA), spectroscopic analyses (FT-IR, UV-Vis ^{1}HNMR, ^{13}CNMR) as well as XRD and SEM techniques. According to the results of numerous analyses, the ligand (HL)interacts with metal ions as a monobasic tridentate chelate. It bonded the metal ions via N atoms of azomethine (Schiff base and imidazole) moieties, and deprotonated hydroxyl oxygen, forming uninuclear metal complexes (M-complexes) with formula $[V(HL)Cl_2(H_2O)].2H_2O$ and $[M(HL)Cl(H_2O)_2].nH_2O$ (where M= Mn(II), n= 2; Co(II), n= 2; Ni(II), n= 4; and Zn(II), n= 0.5.The electronic absorption spectra and magnetic moment measurements of complexes demonstrated that all complexes have an octahedral or distorted octahedral geometry. The XRD results illustrated that the ligand (HL), V(III), and Zn(II) complexes were amorphous, whereas the Mn(II), Co(II), and Ni(II) complexes had monoclinic crystal systems. The TEM results demonstrated that the ligand and Mn(II), Co(II), and Ni(II) complexes were in nano-sized. Thermo gravimetric analysis shows that the complexes disintegrate into four phases at 21-550°C, leaving metal oxide. Disc diffusion and minimum inhibitory concentration (MIC) methods were used to examine the in vitro microbiological activities of the Schiff base and its complexes against *P. aeruginosa, S. aureus, B. subtilis, and E. coli bacteria; C. albicans and A. flavus* fungal strains, respectively. The antimicrobial of the V(III) complex is more effective than the free Schiff base and other complexes. The cytotoxicity of the ligand (HL) and its metal complexes were studied in vitro on WI-38, HepG2, and MCF-7 cell lines by MTT assay. The results showed that the V(III) complex was more potent than the other synthesised compounds against HepG2, and MCF-7 cell lines with IC_{50} values of 18.63±1.5 and 10.50±0.8, respectively.

Keywords: Anticancer, Schiff base, imidazole, antimicrobial activity, metal complexes

INTRODUCTION

The search for innovative antibacterial, antifungal, and carcinoma chemotherapeutics has taken on important significance within the medicinal chemistry field due to the growth of drug-resistant microbe populations. Schiff bases are substances incorporating methyl-imine groups that have biological properties such as being antibacterial, antiviral, and anticancer. Numerous metal complexes of Schiff base could exhibit enhanced biological and catalytic activities because of their powerful capabilities to chelate metallic ions (Hou et al. 2023, Özdemir et al. 2023). Therefore, various Schiff base-based metallic complexes demonstrate unique therapeutic effects. For instance, Ni(II), Cu(II), Mn(II),

Co(III), and Zn(II) Schiff base complexes can activate the tumour suppressor p53 in cancer cells (Shakdofa et al. 2018). Additionally, nitrogen-based heterocyclic substances are a significant and distinctive category of organic substances, they have pharmacological and physiological features (Kerru et al. 2020, P. K. Sharma et al. 2020) as well as being components of many naturally significant molecules, involving several nucleic acids, vitamins, antibiotics, pharmaceuticals, agrochemicals, and dyes, among several others. These compounds cure Alzheimer's disease and have antitumor, free radical scavenging, and anticancer properties (Abdpour et al. 2021, Alikhani et al. 2018, Ramazani et al. 2014, Azizmohammadi et al. 2013, Khoobi et al. 2011a, Khoobi et al. 2011b). Among these heterocyclic molecules is benzimidazole which is also known as 1,3-benzothiazole, benzoglyoxaline, or 1H-benzimidazole. It is a bicyclic substance incorporating a benzene moiety fused to an imidazole moiety that has two nitrogen atoms and is generally utilised as a constructing block in organic synthesis(Wright, 1951, Keri et al. 2015). Benzimidazole derivatives have been found to have low toxicity and are highly effective against several pathogenic strains. They have been attracting and retaining attention over the years due to their diverse biological activities. As a typical heterocyclic ligand, the substantial benzimidazole rings offer the potential for supramolecular recognition through π/π stacking interactions. Additionally, they can serve as both hydrogen bond acceptors and donors, facilitating the assembly of various coordination geometries. At the same time, several benzimidazole derivatives with beneficial pharmacological effects have been found as a result of the incorporation of various substituents around its core structure. Several studies have reported a comprehensive pharmacological framework of benzimidazole and aromatic derivatives with exceptional characteristics (Kantharaju, 2019). Such as antifungal, (Alterhoni et al. 2021), antimicrobial (Alorini et al. 2022, Saeed et al. 2023c, El-Sayed Saeed et al. 2022, Saeed et al. 2023d), antitumor (Suárez-Moreno et al. 2022, Alminderej and Lotfi, 2021) antioxidant (Bhandari et al. 2023), analgesic (Nardi et al. 2023), anti-inflammatory (Patel et al. 2023), antiviral (Porcari et al. 1998), antiulcer (Radhamanalan et al. 2018), antituberculosis (Raghu et al. 2022), antidiabetic (Hayat et al. 2023), anti-Alzheimer (Hussain et al. 2023), antileishmanial (Kumar et al. 2022), antiprotozoal (Escala et al. 2023), anti-convulsant (Chauhan et al. 2023), anti-hypertensive (Zhang et al. 2015), antihistamine (Bodapati et al. 2024), and antimalarial (Mokariya et al. 2023). Additionally, a variety of benzimidazole derivatives have been utilised to shield the skin from ultraviolet rays (Djuidje et al. 2020). Clinically approved benzimidazole drugs include telmisartan, mebendazole, carbendazim, enviradene, candesartan, omeprazole, astemizole, and many more (Brishty et al. 2021). Based on the above information, a new Schiff base ligand incorporating the benzimidazole moiety derivative called, 4-((((1H-benzo[d]imidazol-2-yl)methyl)imino)methyl)benzene-1,3-diol was prepared, and its molecular structure was investigated by ^{1}H-, ^{13}C-NMR, mass, electronic absorption spectra infrared. Then this ligand was utilised to synthesise the Zn(II), Ni(II), Co(II), Mn(II), and V(III) complexes. The structure of the prepared complexes was investigated by analytical, thermal (DTA, TGA), spectroscopic analyses (FT-IR, UV-Vis ^{1}HNMR, ^{13}CNMR) as well as XRD, and SEM techniques. Also, the *in-vitro* microbicides influence of the synthetics was assessed by the disc diffusion and MIC methods versus a group of microorganisms including *P. aeruginosa, S. aureus, B. subtilis, and E. coli, C. albicans,* and *A. flavus strains.* In addition, the cytotoxicity of the synthetics was studied on WI-38, HepG2, and MCF-7 cell lines by MTT assay.

MATERIALS AND METHODS

Experimental

Materials and instruments

1H-benzo[d]imidazol-2-yl)methanamine was purchased from BOC Sciences, while 2,4-dihydroxybenzaldehyde was purchased from Merck. All metal chloride salts were obtained from Loba Chemie, except VCl_3. All solvents and VCl_3 were provided by Sigma-Aldrich. FT-IR data of the ligand (HL) and its M-complexes were collected in the wavenumber range of 400-4000 cm^{-1} using a Cary 600 FT-IR model of the Agilent spectrometer, Santa Clara, USA. The ultraviolet and visible (UV-Vis) spectra of the DMSO solutions of the HL and its M-complexes were scanned in the λ range of 200–1100 nm by a Shimadzu UV-1800 spectrophotometer (Shimadzu, Duisburg, Germany). The ^{1}H and ^{13}C NMR spectroscopies were recorded at 500 MHz on a JEOL model of the JNM-ECA500II spectrometer, Tokyo, Japan, in DMSO-d_6. The XRD patterns of the compounds were obtained by a Rigaku Ultima IV X-ray diffractometer, Tokyo, Japan with Cu Kα radiation (λ = 1.54180 A˚) at a generator voltage of 40 kV and a generator current of 40 mA. The scanning range of 2θ was recorded from 10 ° to 90° with a 0.02 ° step width. The molar conductivities (Λm) of DMSO solutions of the metal complexes were determined at 25°C using Sension + MM374, Loveland, USA at a concentration (1×10^{-3} M). The DTA and TGA were measured under nitrogen by a Shimadzu simultaneous DTA–TG device (DTG-60AH, Japan), with a rate of heating 10 °C /min at a temperature range of 21-550 °C. The DTA measurement reference material was Al_2O_3. Scanning electron microscope (SEM) images were scanned by JEOL JSM-6510LV (JEOL, JSM-6510LV, Japan). JEOL JEM-2100 (JEOL, JEM-2100, Japan) was used to collect the transmission electron microscope (TEM) images. The Stuart SMP-30 was used to measure the melting

points (M.P.) of the samples. The magnetic susceptibility was recorded at 25 °C on Gouy Matthey Balance and determined by the publicised equations (Emam et al. 2020, Al-Hakimi et al. 2023). Elemental analysis (C,H,N, and S) was performed on the samples at Cairo University's Laboratory of Micro-Analytical in Egypt. The chloride and metal ions contents have been evaluated by the Standard analytic techniques (Vogel, 1989, Svehla, 1979).

Synthesis of 4-((((1H-benzo[d]imidazol-2-yl)methyl) imino)methyl) benzene-1,3-diol ligand (HL) (1)

4-((((1H-benzo[d]imidazol-2yl)methyl) imino) methyl) benzene-1,3-diol (HL) was synthesised by refluxing for 5 hrs. a mixture of (1H-benzo[d]imidazol-2-yl)methanamine solution (147 mg, 1 mmol, 30 mL of EtOH) and 2,4-dihydroxybenzaldehyde (138 mg, 1 mmol, 30 mL of EtOH) in the presence of 2 mL of glacial CH_3COOH. The reaction mixture's volume is then decreased to almost 30 mL, and it is allowed to reach room temperature. The matching ligand was produced by drying the green precipitate after it had been washed with ethyl alcohol (HL) (Fig. 1), (245 mg,91.8%). color: green, m.p.=140 °C. Elemental analysis (EA) for $C_{15}H_{13}N_3O_2$ (267.29 g/mol): found (calcd.) %C 67.26(67.40), %H 4.98(4.90), %N 15.47(15.72). FT-IR (cm^{-1}), 3520, 3400, and 3248 ν corresponding to (OH/NH). The bands at 3045w, 2951w, and 2866w refer to ν(C-H). The azomethine group (C=N) showed bands at 1612 and 1603. The bands at 1233 and 1267 refer to ν(C-O). ^{1}H-NMR (500 MHz, DMSO-d_6): δ(ppm): 13.14 (s, 1H, ^{19}OH); 12.73 (s, 1H, ^{9}NH), 10.91 (s,1H, ^{20}OH), 9.93 (s, 1H, N=CH), 6.34-7.53 (m, 7H, Ar-H), 4.33 (s, 2H, CH_2).^{13}C-NMR (150 Mhz, DMSO-d_6): δ(ppm) = 167.52 (C13), 165.25 (C15), 163.30 (C18), 148.16 (C8), 102.26-133.84 (aromatic carbons), 55.35 (C10) ppm.

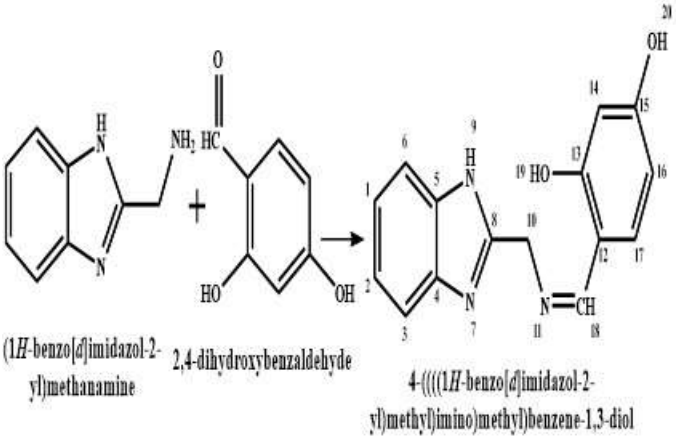

Figure 1: The ligand preparation

Synthesis of metal complexes

Zn(II), Ni(II), Co(II), Mn(II), and V(III) complexes were prepared by mixing the 4-((((1H-benzo[d]imidazol-2-yl)methyl)imino)methyl)benzene-1,3-diol (HL, 1) solution: (276 mg, 1 mmol, in 25 mL/EtOH) with 1 mmol of chloride salts ethanolic solution: $[ZnCl_2].2H_2O$ (172.32 mg), $[NiCl_2].6H_2O$ (237.70 mg), $[CoCl_2].6H_2O$ (237.95 mg), $[MnCl_2].4H_2O$ (197.9 mg), or $[VCl_3].6H_2O$ (265 mg). The reaction mixes were refluxed for 5 hrs. while stirring. The resulting complexes were isolated out rinsed several times with hot EtOH, and eventually dried in a vacuum over $CaCl_2$.

V(III)-Complex:

Yield (49.1%), m.p.>300 °C, colour: dark brown, Λ_m=2.64 $ohm^{-1}cm^2mol^{-1}$, μ_{eff} =2.83 BM. E.A. of $[V(H_2L)Cl_2(H_2O)].2H_2O$, $C_{15}H_{18}Cl_2N_3O_5V$, (442.17 g/mol): Found (calcd.) %C 40.91(40.75), %H 4.05 (4.10), %N 9.05(9.50), %Cl15.81(16.03), %V 11.12(11.52). FT-IR (cm^{-1}) 3449, 3251 ν(OH/NH), 3065w, 2931w, 2856w ν(C-H), 1587 and 1563 ν(C=N), 1240, 1290 ν(C-O), 633 ν(^{19}O-V), 554 ν(^{7}N→V),457 ν(^{11}N→V).

Mn(II)-Complex:

Yield (85%), m.p.=211 °C, colour: brown, Λ_m=14.54 $ohm^{-1}cm^2mol^{-1}$, μ_{eff} =5.91 BM. E.A. of $[Mn(H_2L)Cl(H_2O)_2].2H_2O$, $C_{15}H_{20}ClN_3O_6Mn$, (428.73 g/mol): Found(calcd.) %C 42.35(42.02), %H 4.96 (4.70), %N 10.07 (9.80), %Cl 7.81(8.27), %Mn13.15(12.81). FT-IR (cm^{-1}), 3491, 3230 ν(OH/NH), 3045w, 2900w, 2814w ν(C-H), 1596, and 1555 ν(C=N), 1239,and 1281 ν(C-O), 626 ν(19O-Mn),579 ν(7N→Mn), 418 ν(^{11}N→Mn)

Co(II)-Complex:

Yield (91%), m.p.>300 °C, colour: brown, Λ_m=11.19 $ohm^{-1}cm^2mol^{-1}$, μ_{eff}=4.46 BM. E.A. of $[Co(H_2L)Cl(H_2O)_2].2H_2O$, $C_{15}H_{20}Cl_2N_3O_6Co$, (432.72 g/mol): Found(calcd.) %C 41.89(41.64), %H 4.5.17 (4.66), %N 9.87 (9.71), %Cl 8.01(8.19), %Co 13.77(13.62). FT-IR (cm^{-1}), 3551, 3221 ν(OH/NH), 3033w, 2921w, 2804w ν(C-H), 1595 and 1580 ν(C=N), 1230,and 1276 ν(C-O), 623 ν(^{19}O-Co),547 ν(^{7}N→Co), 424 ν(^{11}N→Co).

Ni(II)-Complex:

Yield (96%), m.p.>300 °C, colour: pale green, Λ_m=7.60$ohm^{-1}cm^2mol^{-1}$, μ_{eff} = 3.18 BM. EA of $[Co(H_2L)Cl(H_2O)_2].4H_2O$, $C_{15}H_{24}ClN_3O_8Ni$, (468.51 g/mol): Found (calcd.) %C 37.89(38.45), %H 5.17 (5.16), %N 8.87 (8.97), %Cl 7.21(7.57), %Ni12.17(12.53). FT-IR (cm^{-1}), 3399, 3244ν(OH/NH), 3070w, 2939w, 2813w ν(C-H), 1599 and 1579 ν(C=N), 1236, and 1283 ν(C-O), 621 ν(^{19}O-Ni),545 ν(^{7}N→Ni), 420 ν(^{11}N→Ni).

Zn(II)-Complex:

Yield (79%), m.p.=254°C, colour: green, Λ_m=7.60 $ohm^{-1}cm^2mol^{-1}$, μ_{eff} = dia. EA of $[Co(H_2L)Cl(H_2O)_2].0.5H_2O$, $C_{15}H_{17}ClN_3O_{4.5}Zn$, (412.15 g/mol): Found(calcd.) %C 44.09(43.71), %H 4.36 (4.16), %N 10.31 (10.20), %Cl 8.21(8.60), %Zn 15.67(15.86). FT-IR (cm^{-1}), 3456, 3231 ν(OH/NH), 3015w, 2971w, 2834w ν(C-H), 1596 and

1561 ν(C=N), 1229, and 1279 ν(C-O), 624 ν(^{19}O-Zn),542 ν(^{7}N→Zn), 455 ν(^{11}N→Zn).

In vitro cytotoxicity activity

Cell culture

In vitro, cytotoxicity activity of the synthetics was tested against three different types of human tumour cell lines; breast cancer line (A549), lung cancer line (MCF-7), and colon cancer line (HCT116). The cells were grown in appropriate media and treated with different concentrations of the synthetics. Cell viability was assessed using a colorimetric assay using a popular method (El-Helby et al. 2019). The results showed dose-dependent cytotoxicity against all three tumour cell lines. These findings suggest that the synthetics have potential as anti-cancer agents and warrant further investigation in preclinical models.

MTT assay

The MTT assay was used to investigate the in vitro cytotoxicity of the synthetics on the cell lines (WI-38, HepG2, and MCF-7) (Mohamad M. E. Shakdofa et al. 2017). Living cells' mitochondrial succinate dehydrogenase converts yellow tetrazolium bromide MTT into a purple formazan derivative in this colorimetric method. The cell lines were seeded in 96-well plates at 1.0x10^{4} cells/well for 48 hours at 37 °C with 5% CO_2. The cells were cultured for 24 hours at various synthetic concentrations. After that, 20 µL of MTT solution at 5 mg/mL was added and incubated for 4 h. Adding 100 µL of DMSO to each well to dissolve the purple formazan. The colorimetric change from purple to yellow indicates the number of viable cells present in each well. The solution's absorbance is measured at 570 nm with a spectrophotometer; and the assay is measured and recorded. The relative cell viability in percentage was calculated. The IC_{50} values were determined (the desired concentration of the tested compound to inhibit cell growth by 50%).

In vitro antibacterial and antifungal activity

The inhibition zone diameter and activity index

By using the disc diffusion method, the synthetics' antibacterial efficacy was evaluated *against G+ (Bacillus subtilis and Staphylococcus aureus), G- (Escherichia coli and Pseudomonas aeruginosa), and fungi (Candida albicans, and Aspergillus flavus)* (Collee et al. 1989, Holder and Boyce, 1994).

Each test was repeated three times. The inhibition zone of the common standard antibiotic "ampicillin" and antifungal "clotrimazole" was also measured using the same method as above at the same concentration and solvent. The activity index % (AI) of the synthetics was estimated by the following formula (Zaky et al. 2011).

$$\textbf{Activity Index}(\%) = \frac{\textbf{Zone of inhibition by test compound (diametre)}}{\textbf{Zone of inhibition by standard (diametre)}} \textbf{x100}$$

The activity index (AI) values were then compared to determine the effectiveness of the synthetic compounds against the tested microorganisms compared with the standard.

Determination of the minimum inhibitory concentration (MIC)

The minimum inhibitory concentration (MIC) of the synthetics against some types of bacteria G+ bacteria such as *B. subtilis S. aureus*, G- bacteria such as *P. aeruginosa and E. coli* and some types of fungi such as *C. albicans*, and *A. flavus* were assessed by the two-fold dilution process. Ampicillin drug was used as the standard in the event for bacteria, and clotrimazole for fungi. The starting concentration of the synthesised compounds is 64 mg.mL^{-1}. Serial diluted solutions were prepared (64, 32, 16, 8, 4, 2, 1, 0.5 mg.mL^{-1}). The MIC values were calculated as the lowest concentration that fully stopped the bacteria from growing visibly (Ahamed et al. 2018).

RESULTS AND DISCUSSION

The condensation of 2,4-dihydroxybenzaldehyde with (1H-benzo[d]imidazol-2-yl)methanamine leads to the formation of 4-((((1H-benzo[d]imidazol-2-yl)methyl)imino)methyl)benzene-1,3-diol ligand (HL) (1), as shown in Fig. 1. Consequently, this ligand interacted with the chloride salts of Zn(II), Ni(II), Co(II), Mn(II), and V(III) in a molar ratio (1M:1HL), leading to the creation of complexes with the subsequent general formulas $[V(HL)Cl_2(H_2O)].2H_2O$ and $[M(HL)Cl(H_2O)_2].nH_2O$ (where M= Mn(II), n=2; Co(II), n=2; Ni(II), n=4 and Zn(II), n=0.5. The prepared compounds' structure was elucidated analytically, thermally, and by several spectroscopical tools, such as UV-Vis., NMR, and FT-IR, as well as mass spectrometry. The postulated molecular formulae were supported by elemental analysis, which also revealed that all complexes formed in a molar ratio (1M:1HL) (Fig. 2). The Zn(II), Ni(II), Co(II), Mn(II), and V(III) complexes are not soluble in organic solvents; methanol, ethanol, acetone, and chloroform but completely soluble in DMSO and DMF. They have molar conductance values ranging from 2.64–14.54 Ω^{-1}mol^{-1}cm^{2}, indicative of the non-electrolyte feature of the complexes, and the Cl^- is connected to the metal ions (Geary, 1971).

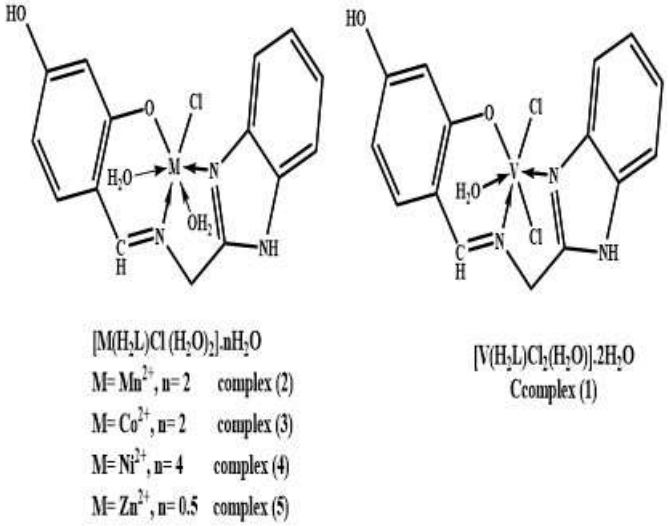

Figure 2: The structure representation of V(III), Mn(II), Co(II), Ni(II), and Zn(II) complexes

Spectroscopical studies

FT-IR Spectra

The FT-IR spectral information of the HL and its M-complexes was described in the experimental section. The very wide band in the 3409-2404 cm^{-1}range may be allocated to the stretching vibration of the NH of the imidazole moiety and hydroxyl groups with intra- and intermolecular H bonding (El-Sayed and Alhakimi, 2022). While the reasonably strong bands observed at 1613 and 1601 cm^{-1} may be allocated to the (C=N) groups of Schiff base and imidazole moieties (Jamil et al. 2023). The medium bands observed at 1233 and 1267 may be ascribed to the phenolic linkages (C-O) (Al.-azab et al. 2022) The coordination mode of Schiff base (HL) (1) can be ascertained by comparing the FT-IR spectra of complexes to those of the unchelated Schiff base (HL) (1). From this comparison, we can conclude that the Schiff base (HL) (1) interacted with different metallic cations in the following mode, it interacted with V(III), Zn(II), Mn(II), Co(II), and Ni(II) as uni-negative tridentate ligand linked covalency of the M ions via the deprotonated OH group (O^{19}) and chelated via the azomethine nitrogen atoms (N^{7} and N^{11}). The following observations served as confirmation of this chelation method;

i) The complexes spectra show a weak band around 3400 cm^{-1} assigned to only one hydroxyl group, indicating the disappearance of the other phenolic hydroxyl groups with a simultaneous positive shift of phenolic (C-O) by 9-23 cm^{-1} (Ahmed N Alhakimi, 2021).

ii) the negative shift in stretching frequency of the azomethine groups of Schiff base and imidazole moieties by 14-26 and 21-46 cm^{-1}.

iii) the emergence of new frequencies of stretching modes of 621- 633, 542-579 and 418-457 cm^{-1}ranges could be inductive to the $\nu(^{19}O\text{-}M)$,$\nu(^{11}N\rightarrow M)$ and $\nu(^{11}N\rightarrow M)$. According to the literature, the asymmetric vibrations (ν_{as}) and symmetric stretching vibrations (ν_s) of the CH_2 group are between 3000 and 2850 cm^{-1}. while the stretching vibrations of CH aromatic are commonly looked at about 3000 cm^{-1}. The ν_s bands of aromatic protons may be responsible for the weak bands observed between 3015 and 3070 cm^{-1}, whereas the weak bands observed between 2921 and 2971 $cm^{-1}$and between 2804 and 2866 cm^{-1} may be attributed to the stretching ν_{as} and ν_s of the methylene group. The boarding in the spectra of all M-complexes in the 3652-2638cm^{-1} range indicates the existence of H_2O which is confirmed by TGA results.

Nuclear magnetic resonance (NMR)

To determine the structure of the Schiff base (HL) and obtain vital information regarding the hydrogen bonding and coordination mechanism with the metal, we need to study the ^{13}C and ^{1}H-NMR spectra. The data from the samples were obtained in DMSO-d_6 and summarised in Section 2.2. In ^{1}HNMR, the vanishing of aldehydic H of the reactant at ≈ 9.9 ppm implies the creation of C=N linkage between the imidazole amino group and the aldehydic group of the 2,4-dihydroxybenzaldehyde reactant. Additionally, the vanishing of aldehydic carbon at ≈190 ppm of the reactant in ^{13}CNMR and its replacement with upfield carbon at 166.31 ensured the creation of an imine moiety in the Schiff base (Shakdofa et al. 2021). In ^{1}HNMR, the compound has three exchangeable protons, at 13.14, 12.73 and 10.91 which are allocated to the protons of the hydroxyl groups of phenolic moieties and the amino group NH of the imidazole moiety. This finding was supported by the fact that their intensity decreased when the solvent was changed from DMSO to DMSO+D_2O, which coincided with the downfield value of C-20 at 166.31 ppm in the benzene ring because of the existence of OH at C-13 and C-15. ^{1}HNMR also indicated the presence of one downfield proton at 9.93, which could be ascribed to the methine proton produced from the imine formation. Additionally, the CH signals overlapped in the 6.43-7.53 ppm range, imputing to the two phenyl rings' aromatic protons. The noted chemical shift of the methylene proton was observed at 4.34 ppm whereas the downfield shift of the singlet peak of H^{14}(7.53), H^{17}(7.47) and the up-filed shift of H^{16} (6.33) suggested the presence of the hydroxyl group at ortho and meta positions for these protons, respectively (Baeva et al. 2013). The ^{1}H-NMR signals of the Zn(II) complex revealed that the chemical shift of only one phenolic hydroxyl proton ($^{13}H\text{-}O^{19}$) disappeared, indicating that the hydroxyl group participated in the metallic ion's chelation in its deprotonated form, which endorsed the proposed chelation mode. The ^{13}C-NMR spectrum of Schiff base showed two chemical shifts of 163.80 and 148.16 ppm which could be assigned to the

azomethine carbons of Schiff base and imidazole moieties (^{18}C&^{8}C) while the chemical shift of C^{13} &C^{15} (δ = 167.52 and 165.25 ppm) demonstrates the presence of a hydroxyl group linked to these carbons. The chemical shifts of aromatic carbons were observed in the 102.26-133.84 range, while the signal appearing at 55.35 ppm could be due to the methylene carbon. The assignment of carbon and protons is confirmed by comparing them with similar compounds (Alhagri et al. 2021).

Magnetic moment (μ_{eff})and electronic absorption spectroscopic (EAS) measurements.

The Schiff base's EAS and that of metallic complexes (2-6) were determined in DMSO, itemised in Table 1, and shown in Figs. 3 and 4. In UV-visible spectrums, Ligand's EAS revealed two distinct sets of bands. The band that appeared at the shortest wavelengths (270 nm) could attributed to the $\pi\rightarrow\pi^*$ transitions, which attributed to the intra-ligand transition in the phenyl moieties (Saeed et al. 2023b). While the two bands at 312 and 389 could be inductive to the $n\rightarrow\pi^*$ transition of C=N groups of Schiff base and imidazole moieties (S. Al-Fakeh et al. 2020). The complexes' n-π^* transitions were shifted somewhat compared to the ligand (HL). This is mostly certainly attributable to the chelation of azomethine-nitrogen with the metallic ions (Saeed et al. 2022). In the hexa-bonded V(III) complex, the ground states $^2T_{2g}$ and ^2E_g split into $^2B_{2g}$, ^2E_g and $^2B_{1g}$, $^2A_{1g}$ respectively. So in an octahedral field there are three spin-allowed transitions corresponding to $^3T_{2g}(d_{xy})\rightarrow{}^3T_{1g}$, $^3A_{2g}(d_{xy})\rightarrow{}^3T_{1g}$, and $^3T_{1g}(P)\rightarrow{}^3T_{1g}$successively (Saeed et al. 2023a). So the peaks that appeared at 490, 625, 995nm, in the EAS of V(III) complex (2) is imputable to the $^2B_{2g}(d_{xy})\rightarrow{}^2E_g(d_{xz},d_{yz})(\nu_1)$, $^2B_{2g}(d_{xy})\rightarrow{}^2B_{1g}(d_{x2-y2})(\nu_2)$ and $^2B_{2g}(d_{xy})\rightarrow{}^2A_{1g}(d_{z2})(\nu_3)$ transition successively. These transitions are consistent with a distorted octahedral structure for V(III) cation (Figs. 3 and 4). This V(III) complex has μ_{eff} value of 2.83 B.M. which is consistent with the d^2 electronic structure of V(III) complexes in an octahedral (Oh)geometry (Lever, 1984). The μ_{eff} value of Mn(II) complex is equal to 5.91 B.M., this value is expected to high spin Mn(II) configuration (d^5) (Anitha et al. 2012). The ground state of the octahedral Mn(II) complex is denoted by the symbol $^6A_{1g}$. Therefore, there are no excited terms for the sextet spin multiplicity, and d–d transitions are prevented in both directions. However, some barred transitions do take place, and as a result, the molar extinction coefficient value of these transitions is quite low. So the EAS of Mn(II) complex expected to display four transitions: $^6A_{1g}\rightarrow{}^4T_{1g}(4G)(\nu_1)$, $^6A_{1g}\rightarrow{}^4E_g(4G)(\nu_2)$, $^6A_{1g}\rightarrow{}^4E_g(4D)(\nu_3)$, and $^6A_{1g}\rightarrow{}^4T_{1g}(4p)(\nu_4)$. The EAS of Mn(II) complex (3) demonstrated four peaks at 630, 541, 510, 470 nm which may be assigned to Mn^{2+}ions in an Oh. geometry (Figs. 3 and 4) (Saeed et al. 2023a).

In Oh geometry, the ^4F ground state of Co(II) can be decomposed into the $^4A_{2g}$, $^4T_{2g}$, and $^4T_{1g}$ states (P), so three spin-allowed transitions $(\nu_1)^4T_1g(F)\rightarrow{}^4T_{2g}(F)$, $(\nu_2)^4T_1g(F)\rightarrow{}^4A_{2g}$and $(\nu_3)^4T_1g(F)\rightarrow{}^4T_{1g}(p)$ are anticipated. So, the presence of three bands at 1071, 675, and 485 nm in the Co(II) complex's EAS indicates that the complex has an Oh geometry.(Fig. 3&4).The ν_1/ν_2 (1.587) low value compared to an Oh Co(II) complex's normal range (1.95-2.48) indicates that this Co(II) complex is distorted. The μ_{eff} of Co(II) complex (4) is 4.46 BM which agrees with the typical value of high spin Oh. Co(II) geometry (El-Tabl et al. 2013).

Table 1: The electronic absorption spectra of Schiff base (HL) and its complexes

Compound	Bands (nm) in DMSO	Electronic transition	μ_{eff} (BM)	Geometry
Schiff base	270, 313, 389	$\pi\rightarrow\pi^*$, $n\rightarrow\pi^*$	--	
V(III) complex	275, 321, 400, 490, 625, 995	$^3T_{2g}(d_{xy})\rightarrow{}^3T_{1g}$ $^3A_{2g}(d_{xy})\rightarrow{}^3T_{1g}$ $^3T_{1g}(P)\rightarrow{}^3T_{1g}$	2.83	Distorted octahedral
Mn(II)complex	269, 323, 434, 470, 510, 541, 630	$^6A_{1g}\rightarrow{}^4T_{1g}$ $^6A_{1g}\rightarrow{}^4E_g$ $^6A_{1g}\rightarrow{}^4E_g$ $^6A_{1g}\rightarrow{}^4T_{1g}$	5.91	
Co(II) complex	276, 327, 399, 485, 675, 1071	$^4T_1g\rightarrow{}^4T_{2g}$ $^4T_1g\rightarrow{}^4A_{2g}{}^4$ $T_1g\rightarrow{}^4T_{1g}$	4.46	

Ni(II) complex	265, 324, 405, 470, 630, 1010	$^3A_{2g}\rightarrow 3T_2g$ $^3A_{2g}\rightarrow {}^3T_{1g}$ $^3A_{2g}\rightarrow {}^3T_{1g}$	3.18	
Zn(II) complex	264, 316, 425	$\pi\rightarrow\pi^*$, $n\rightarrow\pi^*$	Dia	--

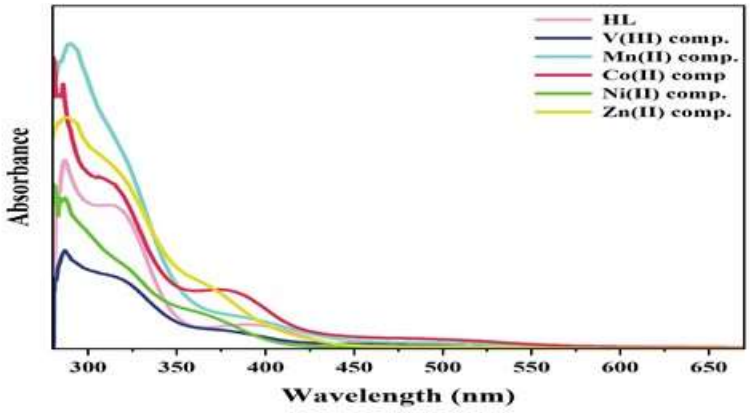

Figure 3: Electronic absorption of ligand and its complexes in the 250-600 nm range

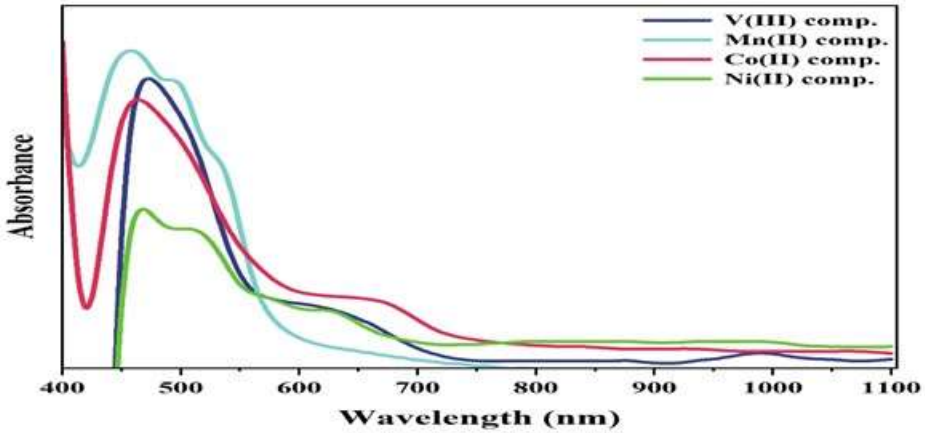

Figure 4: Electronic absorption of complexes in the 400-1100 nm range

The EAS of Ni(II) complex showed three bands at 1010, 518 and 470 nm may be due to the $^3A_{2g}(F)\rightarrow 3T_2g(F)(\nu_1)$, $^3A_{2g}(F)\rightarrow {}^3T_{1g}(F)(\nu_2)$ and $^3A_{2g}(F)\rightarrow {}^3T_{1g}(P)(\nu_3)$ transitions, respectively, which is matched with an Oh. geometry (Figs. 3 and 4) (Lever, 1984, Anitha et al. 2012). The ν_2/ν_1 value is 1.61 which is a typical value for a regular Oh Ni(II) complex (1.5–1.75. The μ_{eff} of Ni^{2+} complex (5) is 3.18 BM which is consistent with a d^8 configuration of Ni(II) complexes in an Oh geometry (Shebl, 2016).

XRD analysis

The XRD patterns of the HL and its M-complexes were examined. The XRD patterns of the ligand, V(III), and Zn(II) complexes show a broad band and did not exhibit any diffraction peaks, which means these compounds are in the non-crystalline (amorphous) phase (Saeed et al. 2014a, Saeed et al. 2014b, Abd El-Hady and Saeed, 2020). In contrast, the XRD patterns of Mn(II), Co(II), and Ni(II) complexes exhibited sharp peaks, indicating that these M-complexes are in the crystalline phase (Farouk et al. 2020, Abd El-Hady et al. 2021). Crystallographic data for these complexes is shown in (Table 2). It was observed that the Mn(II), Co(II), and Ni(II) complexes are in a monoclinic crystal system.

Table 2: The parameters of the unit cell and the crystal data of Mn(II), Co(II), and Ni(II) complexes.

Parameters		Complexes		
		Mn(II)	**Co(II)**	**Ni(II)**
Lattice constant	**a (Å)**	11.200	10.403	6.004
	b(Å)	9.525	7.062	9.328
	c (Å)	6.199	6.640	10.954
Interaxial angle	**α (°)**	90.000	90.000	90.000
	β (°)	99.734	122.021	100.429
	γ (°)	90.000	90.000	90.000
Crystal system		Mono clinic	Mono clinic	Mono clinic
Space group		14 : P121/n1	12 : C12/m1	14 : P121/n1
Unit cell volume (Å3)		651.800	413.560	603.330
Crystal size (nm)		1.580	53.400	43.80

SEM analysis

The SEM technique was used to examine the morphology of HL and its M-complexes. The ligand (HL) exhibited a cluster of spherical shapes of different sizes, as shown in Fig. 5a. These spherical particles have a veined surface shape, as represented in the high-magnification SEM image in Fig. 5b. The morphology of the V(III) complex Fig. 6a exhibits a non-uniform shape. The SEM images of Mn(II), Co(II), and Ni(II) complexes, which are illustrated in Figs. 6b-6d respectively, exhibited a rough surface with a non-uniform shape. The SEM image of the Zn(II) complex Fig. 6e exhibited an irregular rod-like shape in varying sizes. Based on these SEM images, it is noted that the morphology of the ligand is completely different from that of its metal complexes, which indicates that the morphology of the ligand is changed after coordination. Furthermore, the morphology of the complexes differs from each other. It was observed that it changes when metal ions change.

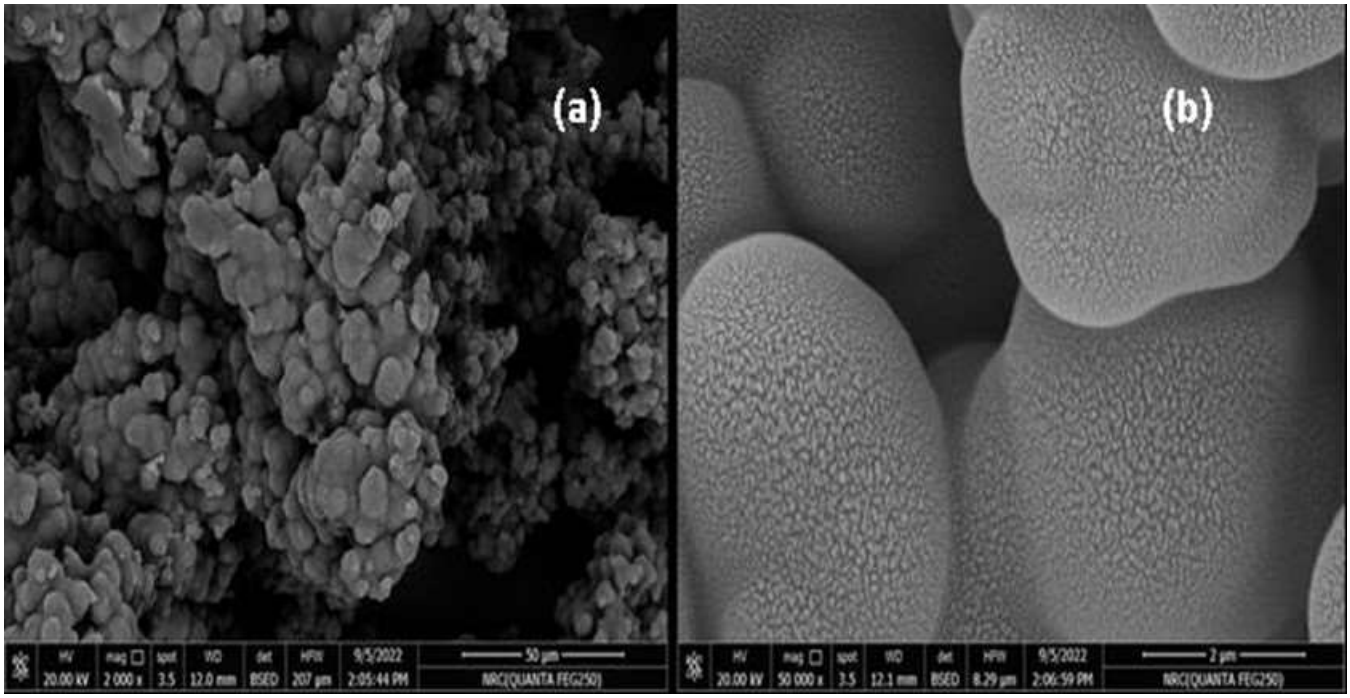

Figure 5: (a) The SEM photos of the HL ligand, (b)The high magnification SEM image of the ligand.

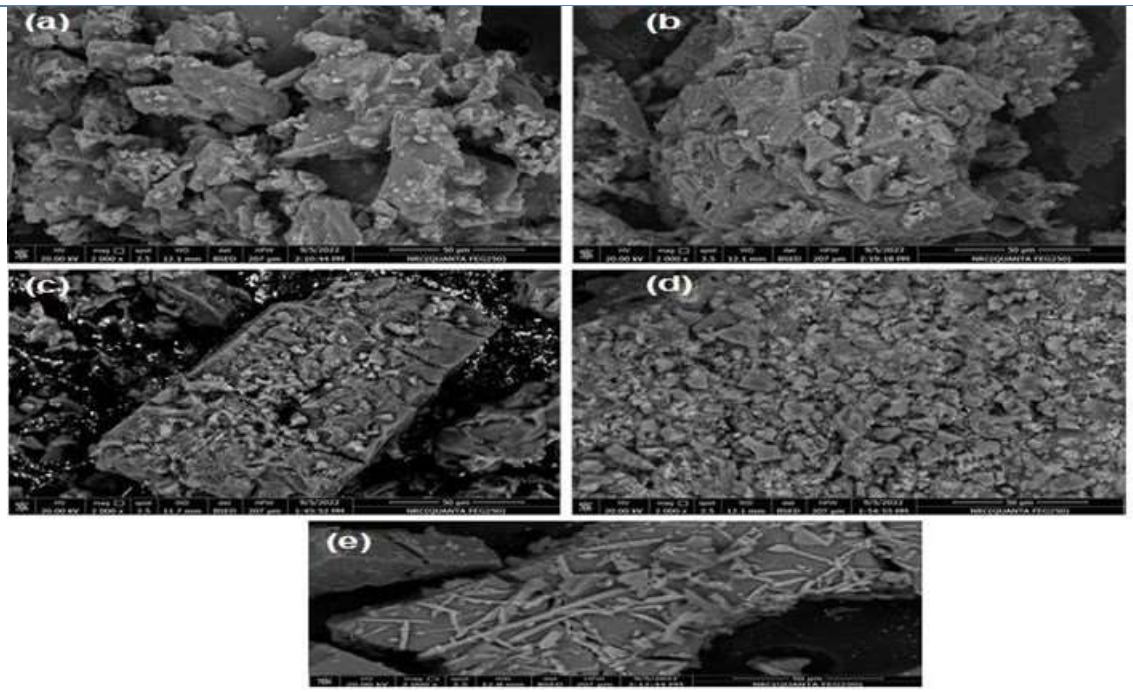

Figure 6: The SEM photos of (a) V(III) complex, (b) Mn(II) complex, (c) Co(II) complex, (d) Ni(II) complex, and (e) Zn(II) complex.

TEM analysis

The TEM technique was applied to investigate the particle size of HL and its M-complexes; Mn(II), Co(II), and Ni(II). The average measurements of the particles were obtained from their TEM images. As shown in (Fig. 7a) the ligand TEM image exhibits agglomerated spherical particles with average diameters of 10.45 nm, and the distribution of its particles is represented in (Fig. 7b). The TEM images of Mn(II) (Fig. 8a), and Ni(II) (Fig. 9a) complexes exhibit agglomerated particles with average diameters of 31.50 and 14.84 nm, respectively. The histogram distribution of the Mn(II) and Ni(II) complexes is represented in Fig. 8b and Fig. 9b, respectively. The TEM image of the Co(II) complex (Figs. 10a and b) displays a star shape. The average of the spike lengths of star particles was 78.57 nm, while the average of the core diameters was 97.18 nm (Fig. 10c), which illustrates the histogram distribution of the spike's lengths of star particles.

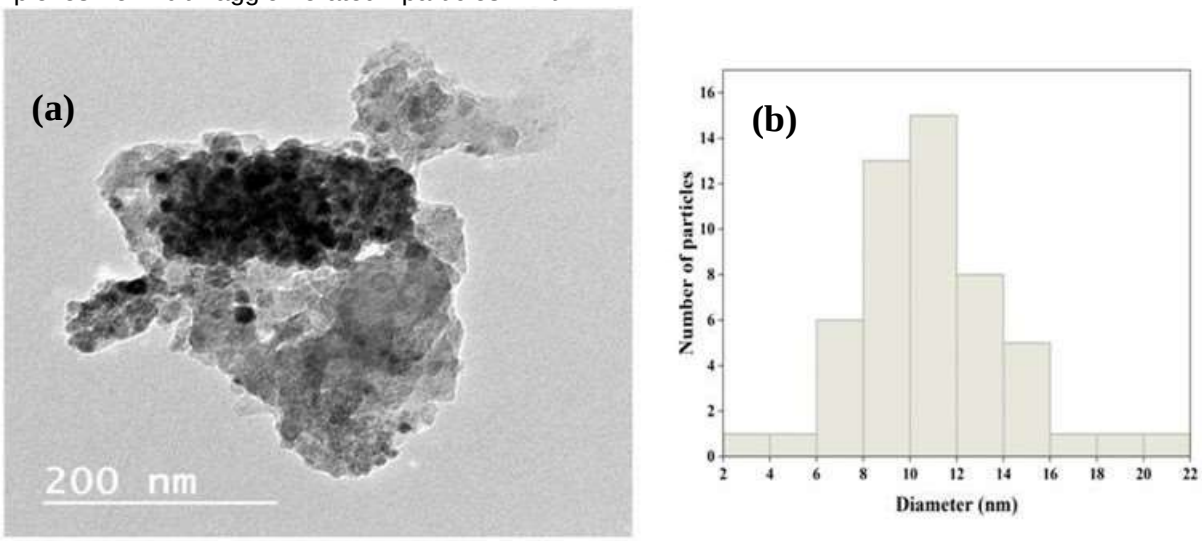

Figure 7: Ligand; (a) High magnification TEM image, (b) The histogram distribution of the nanoparticles.

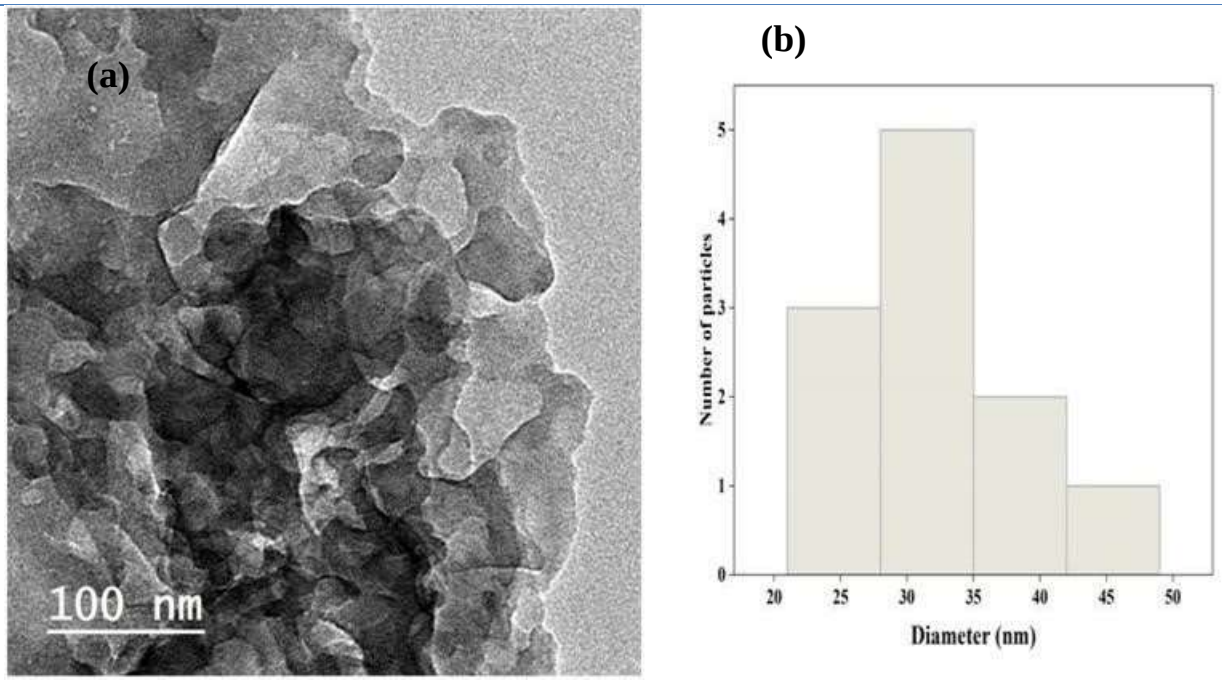

Figure 8: Mn(II) complex;(a) high magnification TEM image, (b) the histogram distribution of the nanoparticles.

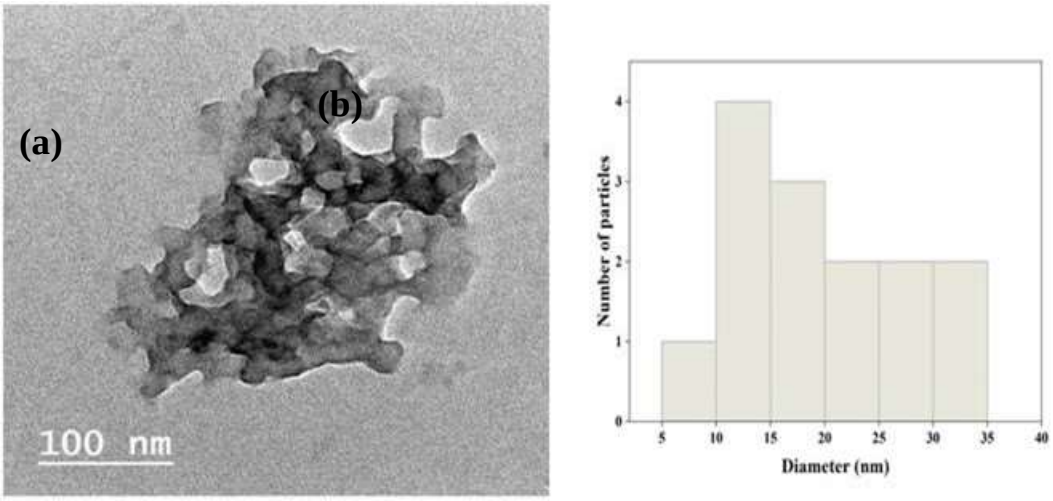

Figure 9: Ni(II) complex; (a) high magnification TEM image, (b) the histogram distribution of the nanoparticles.

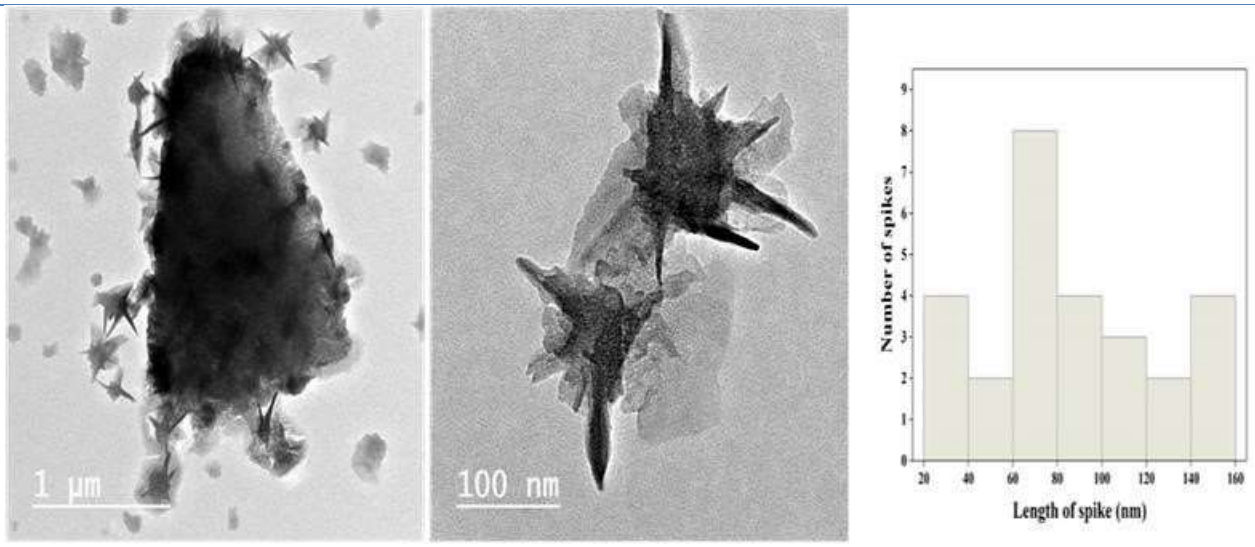

Figure 10: (a) low magnification TEM image of Co(II) complex (b) A high magnification TEM image of the Co(II) complex nanoparticles, (c) The histogram distribution of the spike length of nano-star Co(II) complex.

Thermal analysis

Thermal analyses for complexes ranging in temperature from 25 to 550 ºC have been carried out to gather additional understanding about the nature, composition, and thermal stability of water molecules that are present in M-complexes. The obtained data is summarised in Table 3. The results of the thermal evaluations demonstrated that the recommended formula and the calculation have a mass loss that is compatible with one another. The thermal behaviour of the prepared M-complexes is usually decayed in four stages which can be clarified as follows:

Firstly, the process of dehydration occurred in the 21-141 °C range with weight losses equal to calcd. (found) 8.15(7.92), 8.40(8.43), 8.33(7.87), 15.38(15.00) and 2.19(1.89) % correspondingly. This weight loss is compatible with the elimination of two, four, or half H_2O. Secondly, the elimination of coordinated H_2O molecules which occur in all complexes within the temperature range of 141-215 °C with weight losses ranging from calcd. (found)7.69-8.74 (7.45-8.33) %. This weight loss is the result of the removal of two H_2O molecules that were coordinated with the metal. Thirdly, the elimination of the chloride ions from complex molecules. This process took place at temperatures that varied from 225 to 293 ºC with weight loss equal to16.04(15.77), 8.27(8.00), 8.19(7.88), 7.57(7.13) and 8.60(8.41) % correspondingly. The last stage for all M-complexes occurred in the temperature range of 418-550 °C with weight loss ranging from 47.10-60.73 (46.31-59.65) %. This process, which was accompanied by an exothermic peak, was assigned to the completed decomposition of M-complexes through the departure of the organic portion, which left metal oxide.

Table 3: The data of thermal analysis (TG&DTA) of complexes

compounds	Temp. range ºC	Weight losses	assignment	DTA peaks	
		Found		Endo.	Exo.
V(III) complex	21-141	7.92 (8.15)	Dehydration of $2H_2O$	71	-
	141-275	7.88(8.15)	Elimination of coordinated $2H_2O$	-	-
	225-418	15.77(16.04)	Elimination of 2 Cl^-	411	-
	418-550	46.31(47.10)	Forming V_2O_5	-	467
Mn(II)complex	22-103	8.23 (8.40)	Dehydration of $2H_2O$	101	-
	103-271	8.17 (8.40)	Elimination of coordinated $2H_2O$	171	-
	271-423	8.07(8.27)	Elimination of Cl^-	287	-
	423-550	57.45(58.38)	Forming MnO	-	445
Co(II) complex	21-105	7.92 (8.33)	Dehydration of $2H_2O$	51	-
	105-282	8.39 (8.33)	Elimination of coordinated $2H_2O$	124	-
	282-431	7.97 (8.19)	Elimination of Cl^-	-	-
	431-550	56.71 (57.84)	Forming CoO	-	456

Ni(II) complex	23-75	14.96 (15.38)	Dehydration of $4H_2O$	72	-
	75-316	7.88 (7.69)	Elimination of coordinated $2H_2O$	155	-
	316-483	7.37 (7.57)	Elimination of Cl^-	298	-
	483-550	52.31 (53.42)	Forming NiO	-	488
Zn(II) complex	23-75	1.92 (2.19)	Dehydration of $0.5H_2O$	71	-
	75-316	7.88 (8.74)	Elimination of coordinated $2H_2O$	-	-
	316-483	8.77 (8.60)	Elimination of Cl^-	-	-
	483-550	59.61 (60.73)	Forming ZnO	-	-

Biology studies

In vitro anticancer activities

The cytotoxicity of the synthetics (1-6) was studied in vitro by MTT assay on (MCF-7 (WI-38, and HepG2) cell lines. The IC_{50} values are shown in Fig.11 and recorded in Table 4. By comparing the synthetic samples IC_{50} values with doxorubicin IC_{50} values, it was noted that all the synthetics (1-6) were less potent than doxorubicin. The Zn(II), Ni(II), Mn(II), and V(III) complexes and the ligand exhibited poor cytotoxicity on the WI-38 cell line with IC_{50} range of 54.52±3.1 to 94.63±4.9 µM, while the Co(II) complex had no cytotoxicity on these cell lines. The Mn(II), and Ni(II) complexes exhibited moderate cytotoxicity on the HepG2 cell line, with an IC_{50} values equal to (46.28±2.8 and 27.04±2.1 µM), respectively. In contrast, the Zn(II), Co(II) complexes, and the ligand (HL) demonstrated poor cytotoxicity towards the HepG2 cell line with IC_{50} values equal to (74.39±3.8, 86.24±4.3, and 61.62±3.4 µM), respectively. With IC50 values of (24.931.9), (35.622.3), and (30.872.2 M), respectively, the Ni(II), Mn(II), and ligand (HL) complexes all displayed a moderate cytotoxic effect on the MCF-7 cell line. However, the Zn(II) and Co(II) complexes exhibited poor cytotoxicity toward the MCF-7 cell line, with IC_{50} values equal to (64.07±3.4 and 51.38±3.0 µM), respectively. Among all synthetics **(1-6)**, the V(III) complex had more effective cytotoxicity toward HepG2 and MCF-7 cell lines, with IC_{50} values of (10.50±0.8 µM and 18.63±1.5), respectively.

Table 4: The in vitro cytotoxicity of the ligand (HL) and its M- complexes toward WI-38, HepG2, and MCF-7 cell lines

Compounds	IC50 (µM)*		
	WI-38	HepG2	MCF-7
HL	94.63±4.9	61.62±3.4	30.87±2.2
V(III) complex	63.79±3.7	18.63±1.5	10.50±0.8
Mn(II) complex	54.52±3.1	46.28±2.8	35.62±2.3
Co(II) complex	>100	74.39±3.8	51.38±3.0
Ni(II) complex	71.03±3.9	27.04±2.1	24.93±1.9
Zn(II) complex	76.48±4.2	86.24±4.3	64.07±3.4
Doxorubicin	6.72±0.5	4.50±0.2	4.17±0.2

*** IC_{50} (µM):** 1-10 (very strong); 11-20 (strong); 21-50 (moderate); 51-100 (weak); and greater than 100 (non-cytotoxic) (Alminderej and Lotfi, 2021).

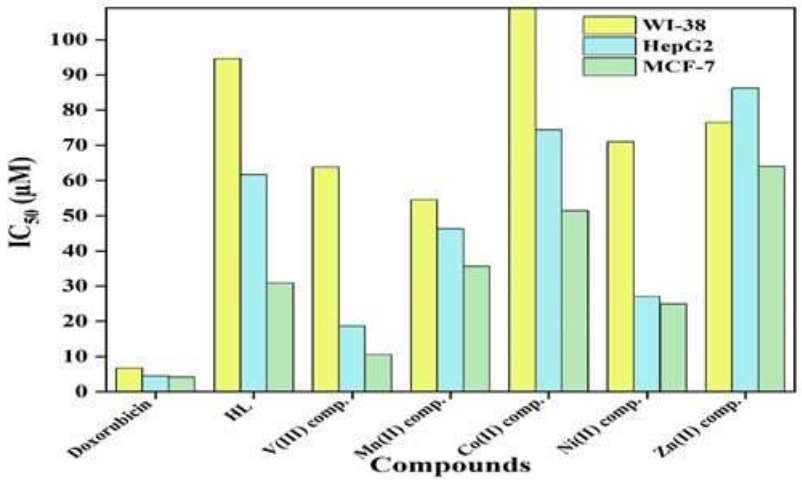

Figure 11: Graphical representation of IC_{50} values of the ligand (HL) and its M-complexes toward MCF-7,HepG2, and WI-38cell lines.

Antimicrobial activities

Disc diffusion method

The results of the microbicidal activity of the synthetics (1-6) towards G^-*(P. aeruginosa and B. subtilis);* G^+*(S. aureus and E. coli); and* Fungi *(C. albicans* and *A. flavus)* were tabulated in Table 5 and Fig. 12-15. The microbicidal activity results showed that all synthetics (1-6) had lower antibacterial activity than the standard drug (ampicillin). Among all the synthesised compounds, the V(III) complex had the highest antibacterial activity against all four selected species of bacteria, with an inhibition zone (IZ) ranging from 11-17 mm and an activity index % (AI) range of 52.4-73.9%. Otherwise, the Zn(II) complex had the lowest antibacterial activity versus *S. aureus, B. subtilis,* and *P. aeruginosa,* and it was inactive against *E. coli.* The order of bactericidal activity of synthetics (1-6) against each bacterial strain is Ampicillin>V(III)>Ni(II)>(HL)>Mn(II)>Co(II))>Zn(II). For antifungal activity, the V(III) complex was more potent than the other synthesised compounds towards *A. flavus* and *C. albicans*. The Zn (II) complex, on the other hand, displayed the lowest fungicidal efficacy against *C. albicans* and *A. flavus*. The order of fungicidal activity of synthetics (1-6) against each fungal strain is clotrimazole>V(III)>Ni(II)> Mn(II)>(HL)>Co(II))>Zn(II).

Table 5: The inhibition zone diameter and activity index of the ligand (HL) and its M-complexes against certain types of bacteria and fungi

Compounds	G+ bacteria				G- bacteria				Fungi			
	S. aureus		*B. subtilis*		*E. coli*		*P. aeruginosa*		*C. albicans*		*A .flavus*	
	IZ (mm)	AI (%)	IZ (mm)	AI (%)	IZ (mm)	AI (%)	IZ (mm)	AI (%)	IZ (mm)	AI (%)	IZ (mm)	AI (%)
HL	9	42.9	11	47.8	8	34.8	11	50.0	14	58.3	9	36.0
V(III) complex	11	52.4	17	73.9	12	52.2	16	72.7	20	83.3	15	60.0
Mn(II) complex	7	33.3	11	47.8	6	26.1	10	45.4	15	62.5	10	40.0
Co(II) complex	5	23.8	8	34.8	3	13.0	7	31.8	10	41.7	7	28.0
Ni(II) complex	10	47.6	14	60.9	8	34.8	13	59.1	19	79.2	13	52.0
Zn(II) complex	3	14.2	6	26.1	NA†	0	5	22.7	8	33.3	5	20.0
Ampicillin	21	100	23	100	23	100	22	100	-	-	-	-
Clotrimazole	-		-	-	-	-	-	-	24	100	25	100

NA† No activity.

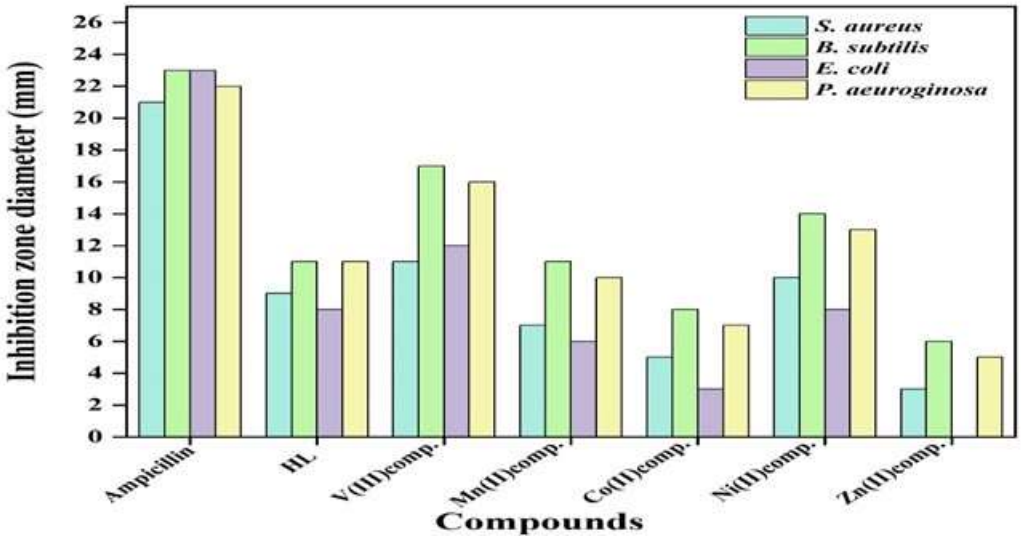

Figure 12: Graphical representation of the inhibition zone diameter of the ligand and its M-complexes against four types of bacteria.

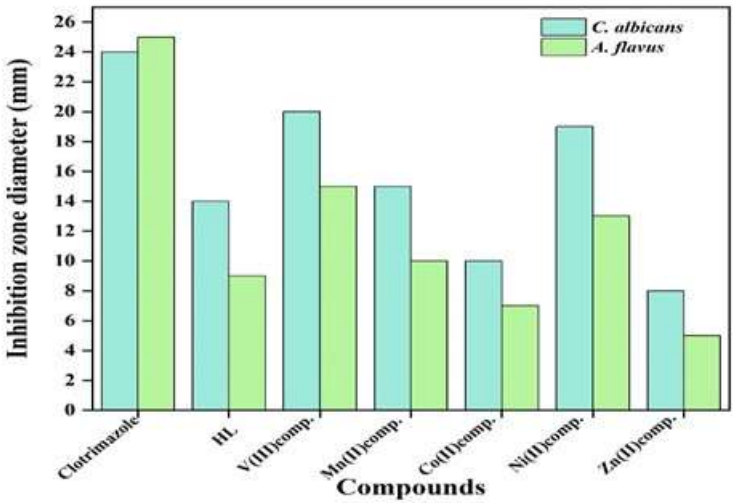

Figure 13: Graphical representation of the inhibition zone diameter of the ligand(HL) and its M-complexes against two types of fungi.

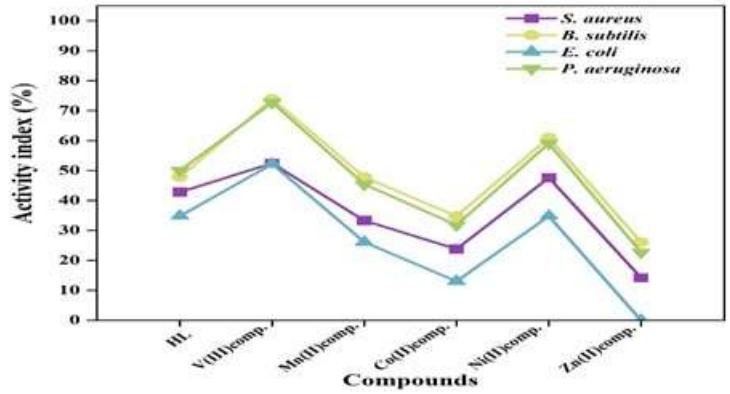

Figure 14: The activity index of the ligand (HL)and its M-complexes against four types of bacteria.

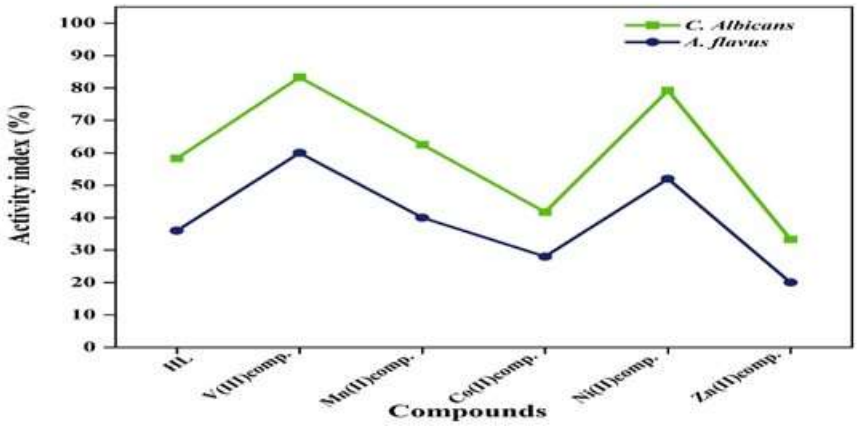

Figure 15: The activity index of the ligand (HL) and its M-complexes against selected species of fungi

Minimum inhibitory concentrations (MICs)

The microbicidal activity of the synthetics (1-6) towards G+ (*S. aureus and B. subtilis);* G- *(E. coli and P. aeruginosa);* fungi *(C. albicans* and *A. flavus*) were assessed by minimum inhibitory concentration. The MIC results displayed in Figs. 16-17 and are recorded in Table 6.

Table 6: The MIC values of the ligand and its M-complexes towards different types of bacteria and fungi.

Compounds	MIC (mg/mL)					
	G+ bacteria		**G- bacteria**		**Fungi**	
	S. aureus	***B. subtilis***	***E. coli***	***P. aeruginosa***	***C. albicans,***	***A. flavus***
HL	32	16	16	16	16	32
V(III) complex	2	4	2	4	2	4
Mn(II) complex	64	32	32	32	8	16
Co(II) complex	64	32	>100	64	32	64
Ni(II) complex	16	8	8	16	4	8
Zn(II) complex	64	64	>100	64	64	64
Ampicillin	1	4	0.5	2	-	-
Clotrimazole	**-**	**-**	**-**	**-**	**2**	**1**

It shows that the MIC values of the synthetics (1-6) against the bacterial and the two fungal strains were within the range of 2-64 mg.mL^{-1}, except for the Zn(II) and Co(II) complexes, which exhibited MIC values >100 mg.mL^{-1} against *E. coli.* The Zn(II) compound was ineffective against the microorganisms *B. subtilis, P. aeruginosa*, and *S. aureus*. The Zn(II) compound was ineffective against the investigated microorganisms, with a MIC value ranged from 64to >100) mg/mL in comparing with that of standard drugs. The Co(II) complex showed poor activity versus *S. aureus, P. aeruginosa,* and *A. flavus,* with MIC values equal to 64 mg.mL^{-1}, and it showed moderate activity versus *B. subtilis* and *C. albicans,* with 32 mg.mL^{-1} MIC compared with the standard drugs. The Mn(II) complex MIC values against all strains varied from poor to good activity. It had poor activity versus *S. aureus* with MIC values equal to 64 mg/mL, moderate activity versus *P. aeruginosa, B. subtilis, E. coli,* and *A. flavus* with MIC values ranging from 16 to 32 mg.mL^{-1}, and good activity versus *C. albicans* with MIC value equal to 8 mg.mL^{-1} compared with the standard drugs. The ligand (HL)exhibited moderate activity versus all microorganisms, with MIC ranging 16 to 32 mg.mL^{-1}. Among all the synthesised compounds, the V(III) complex exhibited good activity, it exhibited MIC values' of 2-4 mg.mL^{-1}range versus *S. aureus*, *P. aeruginosa, E. coli,* and *A. flavus,* and it demonstrated significant activity versus *B. subtilis* and *C. albicans* with MIC values equal to the standard drugs. The Ni(II) complex had moderate activity against *P. aeruginosa* and *S. aureus* with a 16 mg/mL MIC, and it had good activity (MIC equal to 4 to 8 mg.mL^{-1}) versus *C. albicans, B. subtilis, E. coli,* and *A. flavus*.

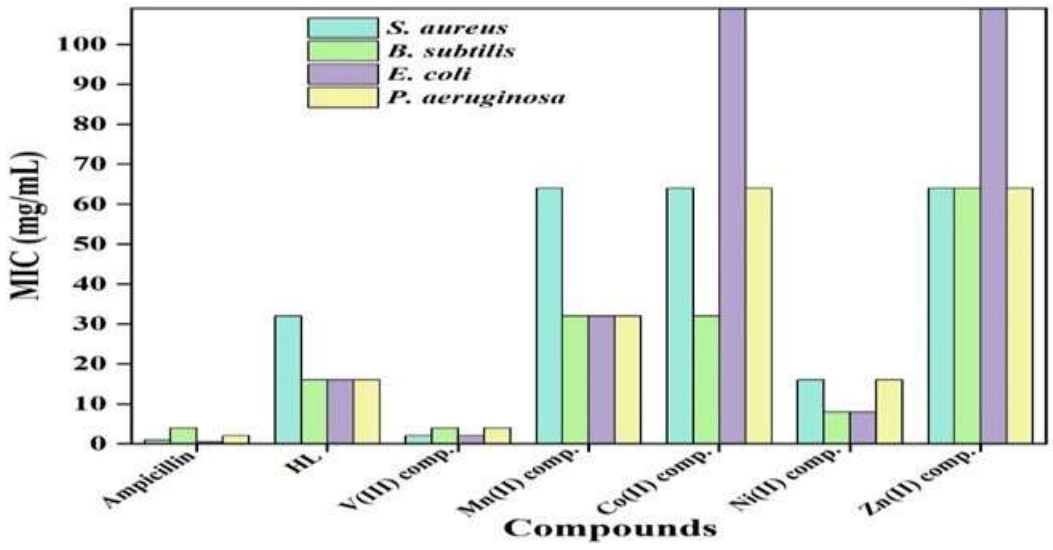

Figure 16: Graphical representation of the MIC values of the ligand (HL) and its M-complexes against different types of bacteria

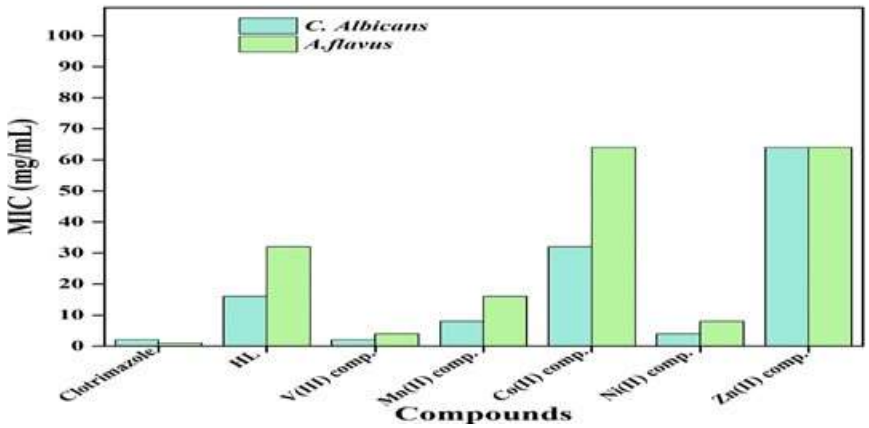

Figure 17: Graphical representation of the MIC values of the ligand (HL) and its M-complexes against two types of fungi

These observations may be attributed to disparities in the cell membrane structures of fungi and yeasts, as well as differences in how these complexes interact with them. Consequently, the microbicidal activity is notably enhanced through the chelation of metallic ions with a ligand (HL). This phenomenon can be elucidated by both Tweedy's chelation theory and the cell permeability, which suggest that due to the pronounced polarity of metallic cations, they face considerable difficulty in traversing the cell membrane (Tweedy, 1964, Benos et al. 1999). However, upon coordination with a ligand (HL), the metal polarity is substantially diminished owing to the overlap between the ligand and metallic orbitals. This leads to a partial neutralization of the metallic positive charge by the donor groups. Furthermore, the lipophilicity of the M-complexes increases as π-electrons become delocalized across the entire chelating ring. Consequently, the M-complex gains easier access to lipid membranes, while the M-complex doing so, it obstructs the metallic binding sites in microbial enzymes.

CONCLUSIONS

One of Schiff's base named 4- ((((1H-benzo[d]imidazol-2-yl)methyl)imino)methyl)benzene-1,3-diol was prepared and characterized using several techniques that together proved its proposed chemical form. Then, its various M-complexes V(III), Mn(II), Co(II), Ni(II), and Zn(II) were prepared and further characterised with several techniques, which in turn also led us to the proposed chemical forms. The prepared compounds showed high effectiveness against some microbes (both bacteria of G+ and G- bacteria, in addition to fungi). The results demonstrated that the V(III) complex is more effective than the free HL (Schiff base ligand) base and the other complexes. As well as some cancer cells, such as lung, colon breast cancer, was studied. The results showed that the V(III) complex was more potent than the other synthesized compounds against HepG2, and MCF-7 cell lines with IC50 with different values. The complexes exhibited poor cytotoxicity on the WI-38 cell line but the V(III) complex had more effective cytotoxicity toward MCF-7 and HepG2 cell lines. The SEM technique shows the ligand (HL) is spherical at different sizes, these spherical particles have a veined surface shape. The morphology of its metal complexes shows a non-uniform shape. Furthermore, the morphology of the complexes differs from each other. It was observed that it changes when metal ions change.

Author contributions

Conceptualization, A. N. Al-Hakemi, T. M. Alresheedi, and S. Saeed; methodology, A. N. Al-Hakemi, T. M. Alresheedi, and R. A. Albarrak ; software, R. A. Albarrak, M. M. Shakdofa, A. E. Albadri, and S. S. Saeed; validation, A. N. Al-Hakemi, T. M. Alresheedi, S. S. Saeed, and M. M. Abd El-Hady; formal analysis, A. N. Al-Hakemi, T. M. Alresheedi, and R. A. Albarrak; investigation, A. N. Al-Hakemi, T. M. Alresheedi, and R. A. Albarrak; data curation, A. N. Al-Hakemi, T. M. Alresheedi, and R. A. Albarrak, M. M. Shakdofa, S. S. Saeed, and M. M. Abd El-Hady; writing-review and editing, J A. N. Al-Hakemi, T. M. Alresheedi, and R. A. Albarrak, M. M. Shakdofa, S. S. Saeed, and M. M. Abd El-Hady; visualization, A. N. Al-Hakemi, T. M. Alresheedi, M. M. Abd El-Hady, and S. Saeed; supervision, A. N. Al-Hakemi and T. M. Alresheedi; project administration, A. N. Al-Hakemi ; funding acquisition, A. N. Al-Hakemi and R. A. Albarrak. All authors have read and agreed to the published version of the manuscript.

Funding statement

There is no funding for this research.

Informed Consent Statement

Not applicable.

Data Availability Statement

All of the data is included in the article.

Conflict of interest

There are no conflicts to declare.

Peer Review: ISISnet follows double blind peer review policy and thanks the anonymous reviewer(s) for their contribution to the peer review of this article.

REFERENCES

Abd el-hady, m. M., farouk, a., saeed, s. E.-s. & zaghloul, s. 2021. Antibacterial and uv protection properties of modified cotton fabric using a curcumin/tio2 nanocomposite for medical textile applications. *Polymers,* 13**,** 4027.

Abd el-hady, m. M. & saeed, s. E.-s. 2020. Antibacterial properties and ph sensitive swelling of insitu formed silver-curcumin nanocomposite based chitosan hydrogel. *Polymers,* 12**,** 2451.

Abdpour, s., jalili-baleh, l., nadri, h., forootanfar, h., bukhari, s. N. A., ramazani, a., ebrahimi, s. E. S., foroumadi, a. & khoobi, m. 2021. Chromone derivatives bearing pyridinium moiety as multi-target-directed ligands against alzheimer's disease. *Bioorganic chemistry,* 110**,** 104750.

Ahamed, a., arif, i. A., mateen, m., surendra kumar, r. & idhayadhulla, a. 2018. Antimicrobial, anticoagulant, and cytotoxic evaluation of multidrug resistance of new 1,4-dihydropyridine derivatives. *Saudi journal of biological sciences,* 25**,** 1227-1235.

Ahmed n alhakimi, m. M. E. S., s el sayed saeed, adel m e shakdofa, maged s al fakeh, ashwaq m abdu, ibrahim a alhagri 2021. Transition metal complexes derived from 2-hydroxy-4-(p-tolyldiazenyl)benzylidene)-2-(p-tolylamino)acetohydrazide synthesis, structural characterization, and biological activities. *Journal of the korean chemical society,* 65**,** 93-105.

Al-hakimi, a. N., alotaibi, m. N. R., al-gabri, n. A. & alnawmasi, j. S. 2023. Biological evaluation of nano-sized novel schiff base ligand-based transition metal complexes. *Results in chemistry,* 6**,** 101107.

Al.-azab, f., jamil, y., al-gaadbi, a., al-hakimi, a., alhagri, i., saeed, s. E.-s. & alhuraishi, e. 2022. Complexes of co(ii), ni(ii) and cu(ii) with 2-((2-methoxybenzylidene)amino) acetohydrazide hydrate: preparation, characterization and antimicrobial activities. *Journal of qassim university for science,* 1**,** 164-185.

Alhagri, i. A., temerk, y. M., al-hazmy, s. M., alhemiary, n. A., alhakimi, a. N. & hassan, m. 2021. Electrochemical reduction and oxidation of the antibiotic cefoxitin-cu2+ complex and its analytical applications. *Chemistryselect,* 6**,** 705-711.

Alikhani, r., razzaghi-asl, n., ramazani, a. & hosseinzadeh, z. 2018. Insights into the structural/conformational requirements of cytotoxic oxadiazoles as potential chemotherapeutic target binding agents. *Journal of molecular structure,* 1164**,** 9-22.

Alminderej, f. M. & lotfi, a. 2021. Design, synthesis, characterization and anticancer evaluation of novel mixed complexes derived from 2-(1h-benzimizadol-2-yl)aniline schiff base and 2-mercaptobenzimidazole or 2-aminobenzothiazole. *Egyptian journal of chemistry,* 64**,** 3351-3364.

Alorini, t. A., al-hakimi, a. N., saeed, s. E.-s., alhamzi, e. H. L. & albadri, a. E. 2022. Synthesis, characterization, and anticancer activity of some metal complexes with a new schiff base ligand. *Arabian journal of chemistry,* 15**,** 103559.

Alterhoni, e., tavman, a., hacioglu, m., şahin, o. & seher birteksöz tan, a. 2021. Synthesis, structural characterization and antimicrobial activity of schiff bases and benzimidazole derivatives and their complexes with cocl2, pdcl2, cucl2 and zncl2. *Journal of molecular structure,* 1229**,** 129498.

Anitha, c., sheela, c. D., tharmaraj, p. & johnson raja, s. 2012. Synthesis and characterization of vo(ii), co(ii), ni(ii), cu(ii) and zn(ii) complexes of chromone based azo-linked schiff base ligand. *Spectrochimica acta - part a: molecular and biomolecular spectroscopy,* 98**,** 35-42.

Azizmohammadi, m., khoobi, m., ramazani, a., emami, s., zarrin, a., firuzi, o., miri, r. & shafiee, a. 2013. 2h-chromene derivatives bearing thiazolidine-2,4-dione, rhodanine or hydantoin moieties as potential anticancer agents. *European journal of medicinal chemistry,* 59**,** 15-22.

Baeva, l. A., biktasheva, l. F., fatykhov, a. A. & lyapina, n. K. 2013. Condensation of acetylacetone with

formaldehyde and thiols. *Russian journal of organic chemistry,* 49**,** 1283-1286.

Benos, d. J., deamer, d. W., kleinzeller, a. & fambrough, d. M. 1999. *Membrane permeability: 100 years since ernest overton*, elsevier science.

Bhandari, s. V., nagras, o. G., kuthe, p. V., sarkate, a. P., waghamare, k. S., pansare, d. N., chaudhari, s. Y., mawale, s. N. & belwate, m. C. 2023. Design, synthesis, molecular docking and antioxidant evaluation of benzimidazole-1,3,4 oxadiazole derivatives. *Journal of molecular structure,* 1276**,** 134747.

Bodapati, a. T. S., reddy, r. S., lavanya, k., madku, s. R. & sahoo, b. K. 2024. Minor groove binding of antihistamine drug bilastine with calf thymus dna: a molecular perspective with thermodynamics using experimental and theoretical methods. *Journal of molecular structure,* 1301**,** 137385.

Brishty, s. R., hossain, m. J., khandaker, m. U., faruque, m. R. I., osman, h. & rahman, s. M. A. 2021. A comprehensive account on recent progress in pharmacological activities of benzimidazole derivatives. 12.

Chauhan, b., kumar, r., mazumder, a., singh, h., yadav, r. K. & abdullah, m. 2023. Updates on the synthetic strategies and structure-activity relationship of anticonvulsant benzothiazole and benzimidazole derivatives. *Letters in drug design & discovery,* 20**,** 1458-1482.

Collee, j., duguid, j., fraser, a. & marmion, b. 1989. Mackie and mccartney practical medical microbiology 5th edition churchill livingstone. Longman groups u. Kltd.

Djuidje, e. N., durini, e., sciabica, s., serra, e., balzarini, j., liekens, s., manfredini, s., vertuani, s. & baldisserotto, a. 2020. Skin damages—structure activity relationship of benzimidazole derivatives bearing a 5-membered ring system. 25**,** 4324.

El-helby, a. A., sakr, h., eissa, i. H., abulkhair, h., al-karmalawy, a. A. & el-adl, k. 2019. Design, synthesis, molecular docking, and anticancer activity of benzoxazole derivatives as vegfr-2 inhibitors. *Arch pharm (weinheim),* 352**,** e1900113.

El-sayed, s. S. & alhakimi, a. N. 2022. Synthesis, characterization of lanthanum mixed ligand complexes based on benzimidazole derivative and the effect of the added ligand on the antimicrobial, and anticancer activities. *Journal of qassim university for science,* 15**,** 35-53.

El-tabl, a. S., shakdofa, m. M. E. & herash, b. M. 2013. Antibacterial activities and spectroscopic characterization of synthetic metal complexes of 4-(3-(hydroxyimino)-4-oxopentan-2-ylidene)amino)-1,5- dimethyl-2-phenyl-1h-pyrazol-3(2h)-one. *Main group chemistry,* 12**,** 257-274.

El-sayed saeed, s., al-harbi, t. M., abdel-mottaleb, m. S., al-hakimi, a. N., albadria, a. E. & abd el-hady, m. M. 2022. Novel schiff base transition metal complexes for imparting uv protecting and antibacterial cellulose fabric: experimental and computational investigations. *Applied organometallic chemistry,* 36**,** e6889.

Emam, s. M., tolan, d. A. & el-nahas, a. M. 2020. Synthesis, structural, spectroscopic, and thermal studies of some transition-metal complexes of a ligand containing the amino mercapto triazole moiety. *Applied organometallic chemistry,* 34**,** e5591.

Escala, n., pineda, l. M., ng, m. G., coronado, l. M., spadafora, c. & del olmo, e. 2023. Antiplasmodial activity, structure–activity relationship and studies on the action of novel benzimidazole derivatives. *Scientific reports,* 13**,** 285.

Farouk, a., saeed, s. E.-s., sharaf, s. & abd el-hady, m. M. 2020. Photocatalytic activity and antibacterial properties of linen fabric using reduced graphene oxide/silver nanocomposite. *Rsc advances,* 10**,** 41600-41611.

Geary, w. J. 1971. The use of conductivity measurements in organic solvents for the characterisation of coordination compounds. *Coordination chemistry reviews,* 7**,** 81-122.

Hayat, s., ullah, h., rahim, f., ullah, i., taha, m., iqbal, n., khan, f., khan, m. S., shah, s. A. A., wadood, a., sajid, m. & abdalla, a. N. 2023. Synthesis, biological evaluation and molecular docking study of benzimidazole derivatives as α-glucosidase inhibitors and anti-diabetes candidates. *Journal of molecular structure,* 1276**,** 134774.

Holder, i. A. & boyce, s. T. 1994. Agar well diffusion assay testing of bacterial susceptibility to various antimicrobials in concentrations non-toxic for human cells in culture. *Burns,* 20**,** 426-429.

Hou, m., li, h. C., an, n., li, w. G. & tong, j. 2023. Synthesis, structure and anticancer studies of cu (ii), ni (ii) and co (ii) complexes based on 2,3-dihydroxybenzaldehyde-2-(2-aminophenyl)benzimidazole schiff base. *Arabian journal of chemistry,* 16**,** 105144.

Hussain, r., khan, s., ullah, h., ali, f., khan, y., sardar, a., iqbal, r., ataya, f. S., el-sabbagh, n. M. & batiha, g. E.-s. 2023. Benzimidazole-based schiff base hybrid scaffolds: a promising approach to develop multi-target drugs for alzheimer’s disease. *Pharmaceuticals,* 16**,** 1278.

Jamil, y., al-azab, f., al-selwi, n., al-duais, f., al-hakimi, a., alhagri, i. & saeed, s. E.-s. 2023. Synthesis, spectroscopic and antibacterial studies of new schiff-base and organophosphorus schiff-base with some transition metal(ii) ions. *Journal of qassim university for science,* 1**,** 129-153.

Kantharaju, k. 2019. Synthesis and pharmacological profile of benzimidazoles. *In:* maria, m. (ed.)

Chemistry and applications of benzimidazole and its derivatives. Rijeka: intechopen.

Keri, r. S., hiremathad, a., budagumpi, s. & nagaraja, b. M. 2015. Comprehensive review in current developments of benzimidazole-based medicinal chemistry. 86**,** 19-65.

Kerru, n., gummidi, l., maddila, s., gangu, k. K. & jonnalagadda, s. B. 2020. A review on recent advances in nitrogen-containing molecules and their biological applications. *Molecules,* 25**,** 1909.

Khoobi, m., emami, s., dehghan, g., foroumadi, a., ramazani, a. & shafiee, a. 2011a. Synthesis and free radical scavenging activity of coumarin derivatives containing a 2-methylbenzothiazoline motif. *Arch pharm chemistry in life sciences,* 344**,** 588-594.

Khoobi, m., foroumadi, a., emami, s., safavi, m., dehghan, g., alizadeh, b. H., ramazani, a., ardestani, s. K. & shafiee, a. 2011b. Coumarin-based bioactive compounds: facile synthesis and biological evaluation of coumarin-fused 1,4-thiazepines. *Chemical biologly drug design,* 78**,** 580-586.

Kumar, a., nimsarkar, p. & singh, s. 2022. Systems pharmacology aiding benzimidazole scaffold as potential lead compounds against leishmaniasis for functional therapeutics. *Life sciences,* 308**,** 120960.

Lever, a. B. P. 1984. *Inorganic electronic spectroscopy,* amsterdam elsevier science.

Mohamad m. E. Shakdofa, el-tabl, a. S., al-hakimi, a. S., wahba, m. A. & morsy, n. 2017. Synthesis, structural characterization and microbicide activities of mononuclear transition metal complexes of 2-(2-hydroxy-5-(p-tolyldiazenyl) benzylidene) hydrazinecarbothioamide. *Ponte,* 73**,** 52-74.

Mokariya, j. A., rajani, d. P. & patel, m. P. 2023. 1,2,4-triazole and benzimidazole fused dihydropyrimidine derivatives: design, green synthesis, antibacterial, antitubercular, and antimalarial activities. *Archiv der pharmazie,* 356**,** 2200545.

Nardi, m., cano, n. C. H., simeonov, s., bence, r., kurutos, a., scarpelli, r., wunderlin, d. & procopio, a. 2023. A review on the green synthesis of benzimidazole derivatives and their pharmacological activities. *Catalysts,* 13**,** 392.

Özdemir, n., karabekmez, f. D., karaca, e. Ö., gürbüz, n. & özdemir, i. 2023. Synthesis, crystal structure, dft studies and catalytic activity of an n-(2,2-dimethyl-1,3-dioxolane-4yl-methyl)benzimidazole ruthenium(ii) hydrate complex. *Journal of molecular structure,* 1281**,** 135159.

P. K. Sharma, a. Amin & m. Kumar 2020. A review: medicinally important nitrogen sulphur containing heterocycles. *The open medicinal chemistry journal,* 14**,** 49-64.

Patel, m., avashthi, g., gacem, a., alqahtani, m. S., park, h.-k. & jeon, b.-h. 2023. A review of approaches to the metallic and non-metallic synthesis of benzimidazole (bnz) and their derivatives for biological efficacy. *Molecules,* 28**,** 5490.

Porcari, a. R., devivar, r. V., kucera, l. S., drach, j. C. & townsend, l. B. 1998. Design, synthesis, and antiviral evaluations of 1-(substituted benzyl)-2-substituted-5,6-dichlorobenzimidazoles as nonnucleoside analogues of 2,5,6-trichloro-1-(β-d-ribofuranosyl)benzimidazole. *Journal of medicinal chemistry,* 41**,** 1252-1262.

Radhamanalan, r., alagumuthu, m. & nagaraju, n. 2018. Synthesis and drug efficacy validations of racemic-substituted benzimidazoles as antiulcer/antigastric secretion agents. 10**,** 1805-1820.

Raghu, m. S., pradeep kumar, c. B., yogesh kumar, k., prashanth, m. K., alshahrani, m. Y., ahmad, i. & jain, r. 2022. Design, synthesis and molecular docking studies of imidazole and benzimidazole linked ethionamide derivatives as inhibitors of inha and antituberculosis agents. *Bioorganic & medicinal chemistry letters,* 60**,** 128604.

Ramazani, a., khoobi, m., torkaman, a., zeinali nasrabadi, f., forootanfar, h., shakibaie, m., jafari, m., ameri, a., emami, s., faramarzi, m. A., foroumadi, a. & shafiee, a. 2014. One-pot, four-component synthesis of novel cytotoxic agents 1-(5-aryl-1,3,4-oxadiazol-2-yl)-1-(1h-pyrrol-2-yl)methanamines. *European journal of medicinal chemistry,* 78**,** 151-156.

S. Al-fakeh, m., amiri, n., n. Al-hakemi, a., el-sayed saeed, s. & e.a.e. albadri, a. 2020. Synthesis and properties of two fe(iii) coordination polymers based on 2-amino-4-methylthiazole, 2-mercaptobenzothiazole and aromatic polycarboxylate. *Asian journal of chemistry,* 32**,** 2502-2506.

Saeed, s., alomari, b. A., alhakimi, a. N., el-hady, a., alnawmasi, j. S., elganzory, h. H. & el-sayed, w. A. 2023a. Pyrimidine hydrazide ligand and its metal complexes: synthesis, characterization, and antimicrobial activities. *Egyptian journal of chemistry,* 66**,** 315-329.

Saeed, s. E.-s., al-harbi, t. M., alhakimi, a. N. & abd el-hady, m. 2022. Synthesis and characterization of metal complexes based on aniline derivative schiff base for antimicrobial applications and uv protection of a modified cotton fabric. *Coatings,* 12**,** 1181.

Saeed, s. E.-s., aldubayyan, m., al-hakimi, a. N. & el-hady, m. M. A. 2023b. Synthesis and characterization of pyridine acetohydrazide derivative for antimicrobial cotton fabric. *Materials,* 16**,** 4885.

Saeed, s. E.-s., alomari, b. A., abd el-hady, m. M. & al-hakimi, a. N. 2023c. Novel pyrimidinethione hydrazide divalent and trivalent metal complexes for improved high-performance antimicrobial and

durable uv blocking cellulosic fabric. *Inorganics,* 11**,** 231.

Saeed, s. E.-s., el-molla, m. M., hassan, m. L., bakir, e., abdel-mottaleb, m. M. S. & abdel-mottaleb, m. S. A. 2014a. Novel chitosan-zno based nanocomposites as luminescent tags for cellulosic materials. *Carbohydrate polymers,* 99**,** 817-824.

Saeed, s. E., abdel-mottaleb, m. M. S. & abdel-mottaleb, m. S. A. 2014b. One-step thermolysis synthesis of divalent transition metal ions monodoped and tridoped cds and zns luminescent nanomaterials. *Journal of nanomaterials,* 2014**,** 873036.

Saeed, s. E. S., aldubayyan, m., al-hakimi, a. N., el-sayed, w. A., alnawmasi, j. S., el-hady, m. M. A. & abdel-mottaleb, m. 2023d. Uv protective textile: experimental and dft computational studies on the function of some metal complexes of hydrazide derivatives on cellulose fabrics. *Applied organometallic chemistry,* 37**,** e7140.

Shakdofa, m. M. E., morsy, n. A., rasras, a. J., al-hakimi, a. N. & shakdofa, a. M. E. 2021. Synthesis, characterization, and density functional theory studies of hydrazone–oxime ligand derived from 2,4,6-trichlorophenyl hydrazine and its metal complexes searching for new antimicrobial drugs. *Applied organometallic chemistry,* 35**,** e6111.

Shakdofa, m. M. E., mousa, h. A., labib, a. A., abd-el-all, a. S., el-beih, a. A. & abdalla, m. M. 2018. Synthesis and characterization of novel chromone schiff base complexes as p53 activators. *Applied organometallic chemistry,* 32**,** e4345.

Shebl, m. 2016. Mononuclear, homo- and hetero-binuclear complexes of 1-(5-(1-(2-aminophenylimino)ethyl)-2,4-dihydroxyphenyl)ethanone: synthesis, magnetic, spectral, antimicrobial, antioxidant, and antitumor studies. *Journal of coordination chemistry,* 69**,** 199-214.

Suárez-moreno, g. V., hernández-romero, d., garcía-barradas, ó., vázquez-vera, ó., rosete-luna, s., cruz-cruz, c. A., lópez-monteon, a., carrillo-ahumada, j., morales-morales, d. & colorado-peralta, r. 2022. Second and third-row transition metal compounds containing benzimidazole ligands: an overview of their anticancer and antitumour activity. *Coordination chemistry reviews,* 472**,** 214790.

Svehla, g. 1979. *Vogel's textbook of macro and semi micro quantitative inorganic analysis,* new york, longman inc.

Tweedy, b. G. 1964. Plant extracts with metal ions as potential antimicrobial agents. *Phytopathology,* 55**,** 910–914.

Vogel, a. I. 1989. Vogle's text book of quantitative chemical analysis. 5th ed. New york: john wiely & sons

Wright, j. B. 1951. The chemistry of the benzimidazoles. *Chemical reviews,* 48**,** 397-541.

Zaky, r. R., ibrahim, k. M. & gabr, i. M. 2011. Bivalent transition metal complexes of o-hydroxyacetophenone [n-(3-hydroxy-2-naphthoyl)] hydrazone: spectroscopic, antibacterial, antifungal activity and thermogravimetric studies. *Spectrochimica acta - part a: molecular and biomolecular spectroscopy,* 81**,** 28-34.

Zhang, y., xu, j., li, y., yao, h. & wu, x. 2015. Design, synthesis and pharmacological evaluation of novel no-releasing benzimidazole hybrids as potential antihypertensive candidate. 85**,** 541-548.